NANO LETTERS

Letter

pubs.acs.org/NanoLett

Ultrasensitive Optical Shape Characterization of Gold Nanoantennas Using Second Harmonic Generation

Jérémy Butet,* Krishnan Thyagarajan, and Olivier J. F. Martin

Nanophotonics and Metrology Laboratory (NAM), Swiss Federal Institute of Technology Lausanne (EPFL), 1015, Lausanne, Switzerland

Supporting Information

ABSTRACT: Second harmonic generation from plasmonic nanoantennas is investigated numerically using a surface integral formulation for the calculation of both the fundamental and the second harmonic electric field. The comparison between a realistic and an idealized gold nanoantenna shows that second harmonic generation is extremely sensitive to asymmetry in the nanostructure shape even in cases where the linear response is barely modified. Interestingly, minute geometry asymmetry and surface roughness are clearly revealed by far-field analysis, demonstrating that second harmonic generation is a promising tool for the sensitive optical characterization of plasmonic nanostructures. Furthermore, defects located where the linear field is strong (e.g., in the antenna gap) do not necessarily have the strongest impact on the second harmonic signal.

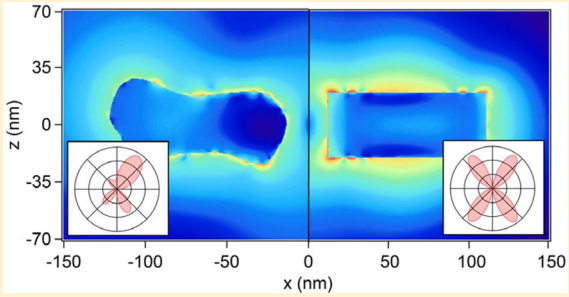

KEYWORDS: *Plasmonics, nonlinear optics, surface integral formulation, realistic nanostructures*

Metallic nanostructures supporting surface plasmon resonances (SPR), that is, collective excitations of the conduction electrons, exhibit unique optical properties.[1] Furthermore, the coupling between several substructures is a convenient way to control SPR properties.[2,3] In particular, bringing two nanostructures in close proximity results in an enhancement by several orders of magnitude of the electric field in the hot spot. This geometry is called a nanoantenna, or an optical antenna, since it represents the optical analogous of microwave and radiowave antennas.[4−6] The electromagnetic properties of nanoantennas can be tuned by modifying their geometric parameters (length, shape, and gap dimension) and tailored for specific applications.[7] For instance, optical antennas have been designed for studying quantum systems at the single emitter level,[8−10] surface-enhanced Raman scattering,[11−13] beamed Raman scattering,[14] cathodoluminescence,[15] strong-field photoemission,[16] and trapping.[17,18]

Optical antennas are also promising for the observation of nonlinear optical effects that require a high electric field such as that observed in the hot spots.[19] Several studies have reported the observation of multiphoton excited luminescence,[20−22] second harmonic generation (SHG),[23,24] third harmonic generation,[25,26] high harmonic generation,[27] and four-wave mixing,[28] as well as ultrafast spectroscopy.[29,30] Recently, a new approach has been proposed to enhance nonlinear conversion in nanoantennas, using structures that are resonant at the several wavelengths involved in the frequency conversion.[31−33] Among the different nonlinear parametric optical processes, SHG is the simplest one and has the advantage of being sensitive to the symmetry of the plasmonic nanostructures as well as their spatial arrangement.[34−40] Contrary to the other nonlinear optical processes, it was observed that SHG can be significantly suppressed in centrosymmetric gaps, although the fundamental electric field is strongly enhanced.[41] On the other hand, efficient SHG is observed in asymmetric gaps, such as the one formed in noncentrosymmetric T-shaped gold dimers.[42] A clear insight into the impact of the nanoantenna shape on their SHG properties, particularly in the far-field, is therefore required to guide further the development of SHG from nanoantennas for practical applications like nonlinear plasmonics sensing.[43]

In this Letter, we compare the linear and second harmonic (SH) optical responses of two gold nanoantennas. We consider an idealized nanoantenna with rectangular shape arms and a realistic nanoantenna obtained from a scanning electron microscope image.[44] While in the linear regime both kinds of nanoantennas have the same emission pattern, this is not anymore the case for their SH response. Furthermore, although the SH near-field distributions appear almost identical at the first sight, the SH far-field distributions of the realistic nanoantenna strongly differ from that of the idealized structure. Further investigations show that geometric defects, such as arm misalignments and tilts, are also clearly revealed in SH far-field distributions. These results demonstrate that SHG can be an extremely sensitive optical tool for the characterization of the geometry of plasmonic nanostructures.

Received: January 30, 2013
Revised: March 1, 2013
Published: March 4, 2013

   dx.doi.org/10.1021/nl400393e | *Nano Lett.* 2013, 13, 1787−1792

The linear optical response of both ideal and realistic nanoantennas has been numerically computed using an in-house surface integration equation (SIE) code giving accurate results for both the near and the far field distributions, even in resonant conditions.[45,46] Dispersive gold dielectric constants used in this work are obtained from experimental data and the optical antennas are considered in vacuum.[47] The case of the idealized nanoantenna is discussed first. The nanoantenna is composed of two 40 nm × 40 nm × 98.5 nm rectangular arms separated by a 25 nm gap. For such dimensions, the dipolar scattering longitudinal resonance of the nanoantenna is superposed to that of the realistic nanoantenna discussed below.[44] Figure 1 shows the near-field intensity distribution and

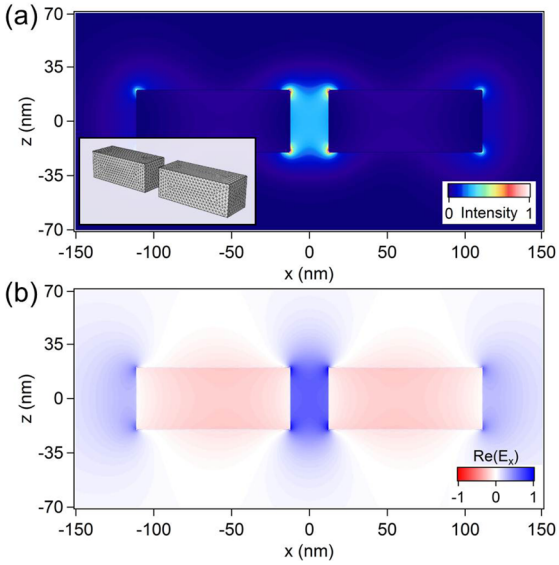

Figure 1. (a) Near-field distribution of the fundamental intensity close to an idealized gold nanoantenna. The arm dimensions are 40 nm × 40 nm × 98.5 nm and the gap dimension is 25 nm. The inset shows the mesh used for the computation. The excitation wavelength is 630 nm corresponding to the maximum of the scattering cross section. (b) The real part of the x-component of the fundamental electric field Re(E_x) evaluated under the same conditions.

the real part of the x-component of the electric field at the fundamental wavelength computed for an incident wave propagating along the y-direction and polarized along the x-direction. The excitation wavelength is 630 nm, corresponding to resonant excitation. As expected, a strong enhancement of the electric field inside the nanogap and a symmetrical electric field distribution are observed (Figure 1b). As discussed in the introduction, the nanoantenna shape modifies its optical response and the properties of realistic and idealized nanoantennas are expected to be different.[7,44] Contrary to the idealized nanoantenna, the surface of the realistic nanoantenna is no longer flat and is a good example of surface roughness occurring in fabricated nanostructures (see the inset Figure 2a). Figure 2 shows the near-field distribution of both the fundamental intensity and the real part of the x-component of the fundamental electric field Re(E_x), computed for the realistic structure and considering identical illumination conditions to the ideal antenna. Note that the phase of imaginary quantities is defined relatively to that of the incident field at the origin, which is pure real quantity (t = 0). The comparison with the ideal case shows that the general features

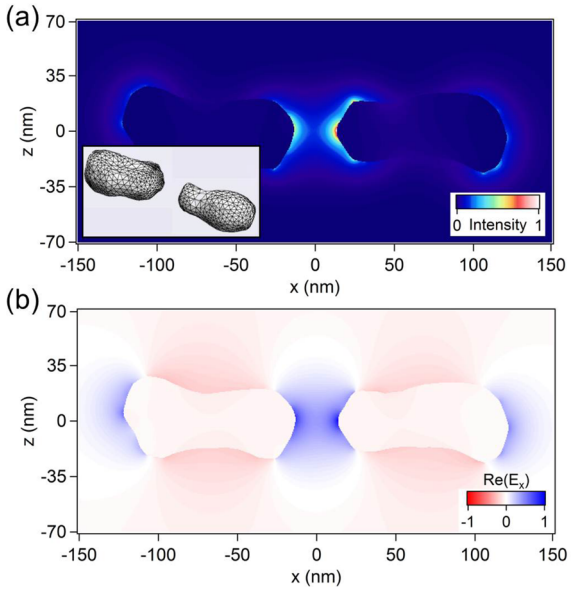

Figure 2. (a) Near-field distribution of the fundamental intensity close to a realistic gold nanoantenna. The mesh was adapted from a scanning electron microscope image (see inset).The excitation wavelength is 630 nm corresponding to the maximum of the scattering cross section and (b) the real part of the x-component of the fundamental electric field Re(E_x) evaluated under the same conditions.

of these distributions, namely an electric field intensity enhancement in the gap of the order of 100 at the gap center and a constant sign for Re(E_x) across the nanogap, are identical. Near-field distributions are very challenging to measure experimentally, while scattered intensities are easily recorded with optical microscopes if the scattering cross section is not too low. The scattered intensities calculated considering the scattered wave polarized into the (O, x, y) plane are shown in Figure 3 as a function of the scattering angle for both the

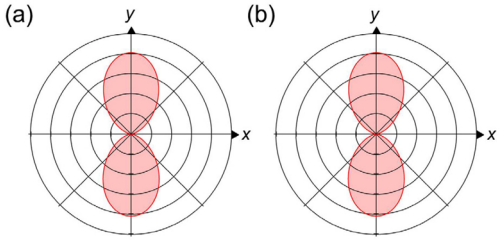

Figure 3. Normalized scattered intensity as a function of the scattering angle calculated considering the scattered wave polarized in the (O, x, y) plan in the case of (a) idealized and (b) realistic nanoantennas. The incident wave propagates along the y-axis and is polarized along the x-axis. The meshes used are identical to the ones used for Figures 1 and 2.

idealized (Figure 3a) and the realistic (Figure 3b) nanoantennas. In both cases, a two lobe pattern, characteristic of a dipolar emission, is observed. These results indicate that linear optical processes do not provide any information on the exact detailed structure of the nanoantennas. We will see below that the impact of the nanoantenna morphology is much stronger in the nonlinear case.

Let us now consider the SH optical response of both gold nanoantennas. It is well-known that SHG is forbidden in the bulk of centrosymmetric media within the dipolar approx-

dx.doi.org/10.1021/nl400393e | Nano Lett. 2013, 13, 1787−1792

imation.[48] Nevertheless, this symmetry is broken at the interface between two centrosymmetric media and SHG arises from metallic nanostructure surfaces. SIE methods only require the discretization of the surfaces of the metal nanoparticles, exactly where the SHG sources are located, and are therefore extremely well suited for the accurate SHG computation, as recently demonstrated by Kauranen and colleagues.[49] Surface SHG computation has been implemented in our SIE code following the method described in ref 49, which is briefly outlined here. First, the linear surface currents, which are expanded on Rao−Wilton−Glisson (RWG) basis functions,[45] are used for the evaluation of the fundamental electric fields just below the gold surfaces and then used for the calculation of the surface SH polarization. We consider only the component $\chi_{surf,nnn}$ of the surface tensor, where n denotes the component normal to the surface, which is known to dominate the surface response for metallic nanoparticles.[50] Note that other contributions to the SH signal, namely the component $\chi_{surf,ttn}$ of the surface tensor (where t denotes the component tangential to the surface) and bulk contribution, are theoretically allowed but these contributions weakly contribute to the total SHG.[50,51] In the present case, the nonlinear polarization can be written as $P_{surf,n}(r,2\omega) = \chi_{surf,nnn}E_n(r,\omega)E_n(r,\omega)$. The SH surface currents are obtained solving the SIE formulation taking into account the nonlinear polarization and enforcing the boundary conditions at the nanostructure surfaces.[49] As the linear surface currents, the SH surface currents are expanded on RWG basis functions. The expansion coefficients are found applying the method of moments with Galerkin testing.[45] A Poggio−Miller−Chang−Harrington−Wu formulation is used to ensure accurate solutions even at resonant conditions.[45,49] The SH electric field is then deduced from the SH surface currents using a two-term subtraction method for the evaluation of the Green functions.[45] The robustness of our program has been tested by comparing with previous experimental results, finite elements calculations and nonlinear Mie theory.[34,52] Our results are found to be very accurate, except for the extreme near-field (distance from the metallic surface below 5 nm). The discrepancy in the extreme near-field is not surprising since the nonlinear polarization is represented by piecewise constant functions.[49] This SIE code offers the possibility to include several embedded domains as required for the description of nanoantennas.[44,45]

As for the linear response, the case of an idealized dipole nanoantenna is considered first. Figure 4 shows the near-field distribution (logarithmic scale) of the SH intensity driven by an incident wave (λ = 630 nm) propagating along the y-axis and polarized along the x-axis. Contrary to the linear case, the SH electric field is not especially enhanced in the gap between both arms. This result, surprising at first sight, is easily understood with the intrinsic properties of SHG in mind. The idealized dipole nanoantenna has a perfectly centrosymmetric shape, which leads to a perfectly centrosymmetric SH electric field distribution (Figure 4b). In order to preserve the centrosymmetry of the problem under study, the SH electric field at each sides of the nanogap must oscillate out of phase, leading to a minimal amplitude of the x-component of the SH electric field along the x = 0 axis because of destructive interferences.[41] Note that this strongly differs from the linear response for which the electric field at opposite sides of the nanogap oscillates in phase (see Figure 1). Indeed, the SH intensity minimum at the gap center indicates a nonradiative behavior, that is, a SH dark mode weakly coupled to the far-field.[41] Note that efficient SH

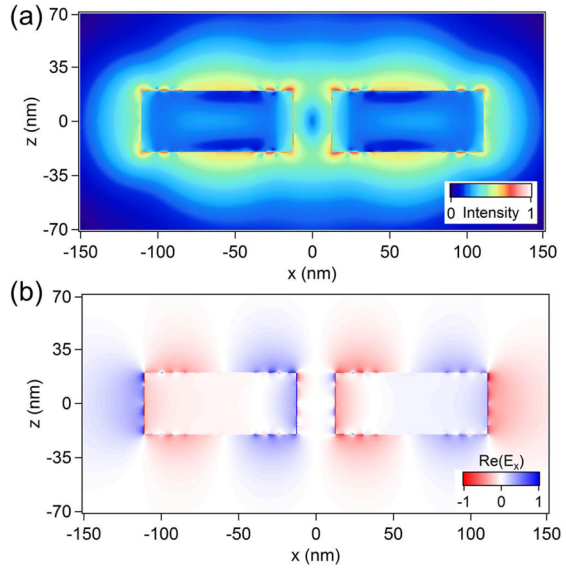

Figure 4. (a) Near-field distribution of the second harmonic intensity (shown in a logarithmic scale) close to an idealized gold nanoantenna. The arm dimensions are 40 nm × 40 nm × 98.5 nm and the gap dimension is 25 nm. The excitation and second harmonic wavelengths are equal to 630 and 315 nm respectively. (b) The real part of the x-component of the second harmonic electric field Re(E_x) evaluated under the same conditions.

dipolar emission from noncentrosymmetric nanoparticles is allowed.[36] This underlines the role played by symmetry in the SHG from nanoantennas.

Let us now consider the realistic antenna. Figure 5 shows the near-field distribution of the SH intensity close to a realistic gold nanoantenna. The mesh used is identical to the one used

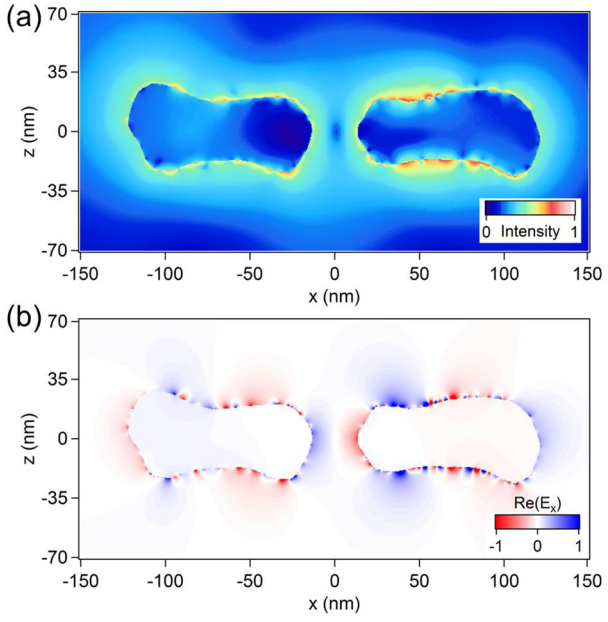

Figure 5. (a) Near-field distribution of the second harmonic intensity (shown in a logarithmic scale) close to a realistic gold nanoantenna. The mesh used is identical to the one used for Figure 2. The excitation and second harmonic wavelengths are equal to 630 and 315 nm, respectively. (b) The real part of the x-component of the second harmonic electric field Re(E_x) evaluated under the same conditions.

dx.doi.org/10.1021/nl400393e | Nano Lett. 2013, 13, 1787−1792

in Figure 2. The fundamental and SH wavelengths are again 630 and 315 nm, respectively. The SH electric field distribution around the nanoantenna is not as symmetric as in the realistic case but similarities are however observed. For instance, the sign of the SH electric field changes across the nanogap and the SH intensity minimum inside the gap is also observed, as was the case for the idealized structure. Previously, we have observed that in the far-field the linear emission patterns are identical for both the idealized and the realistic nanoantennas. This is not anymore the case for the SHG emission pattern, as is visible in Figure 6, which shows the normalized scattered SH

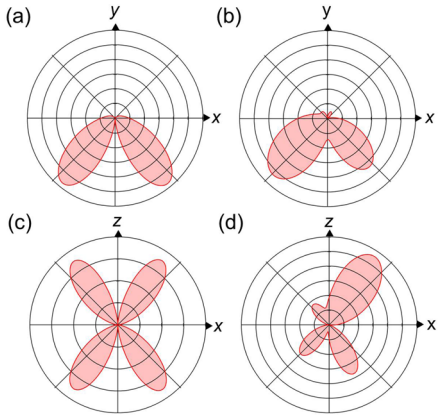

Figure 6. Normalized second harmonic intensity scattered in the horizontal plane as a function of the detection angle calculated considering the second harmonic scattered wave polarized in the (O, *x*, *y*) plane in the case of the (a) idealized and (b) realistic nanoantennas and scattered in the vertical plane calculated considering the second harmonic scattered wave polarized into the (O, *x*, *z*) plane in the case of the (c) idealized and (d) realistic nanoantennas. The fundamental wave propagates along the *y*-axis and is polarized along the *x*-axis. The meshes used are identical to the ones used for the near-field computations.

intensity as a function of the detection angle calculated for both nanoantennas. Contrary to the linear scattering, the emission patterns are completely different. In the case of the idealized nanoantenna, two symmetric lobes are observed in the horizontal plane (O, *x*, *y*) and both the backward and forward SH intensities vanish, as expected for centrosymmetric plasmonic nanostructures.[53] The four lobe pattern observed in the vertical plane is characteristic of a quadrupolar emission, Figure 6c. The observation of a higher multipolar mode is not surprising since SHG from centrosymmetric nanostructures is forbidden in the dipolar approximation.[52,53] On the other hand, the SH wave scattered by the realistic optical antenna is clearly asymmetric, in correlation with the asymmetric nanoantenna arm shapes. For example, the magnitudes of the two lobes observed in the horizontal plane differ by almost 20% and the magnitudes of the four lobes observed in the vertical plane differ by a factor of 3. Furthermore, the SH intensity scattered along the *y*-direction does not vanish anymore since the centrosymmetry is broken. Contrary to the case of individual metal nano-objects,[39] morphology sensitive SHG from nanoantennas does not require cylindrical vector beam excitation but is observed even when the nanoantenna is driven by a plane wave.

In order to investigate further the impact of surface roughness on the SHG from nanoantennas, several computations have been performed adding a protruding defect to the idealized nanoantenna at different positions (see Supporting Information Figures S1−S3).[54] The results show that the impact on the SH far-field is higher in the case of a defect on the lateral arm side than in the case of a defect in the gap, despite the strong fundamental field enhancement in the gap. This somewhat counterintuitive result is easily understood having in mind that SHG from the nanogap is not efficiently radiated to the far-field due to destructive interferences (see the case of the perfect antenna, Figure 4).[41,42] On the other hand, the contribution of a defect on the lateral arm side does not suffer from this limitation and has a stronger impact on the SH far-field (compare Supporting Information Figure S2a with Figure S2b). Further simulations have been performed considering nanodefects on each arm of the idealized nanoantenna (Supporting Information Figure S4). They demonstrate that the symmetry of the nanodefects positions is revealed by the SH far field (Supporting Information Figure S4e and S4f). Asymmetry in the arm shape is not the only defect observed in realistic antennas. Arm tilts and misalignments can also occur during the fabrication process. Let us first consider the case of arm tilts. The right arm of the idealized antenna is turned around the (O_1, *y*)-axis by an angle α (Figure 7a). The normalized SH intensity scattered in the vertical plan as a function of the detection angle calculated considering the SH scattered wave polarized into the (O, *x*, *z*) plane is shown for different values of the rotation angle α (Figure 7b). As the

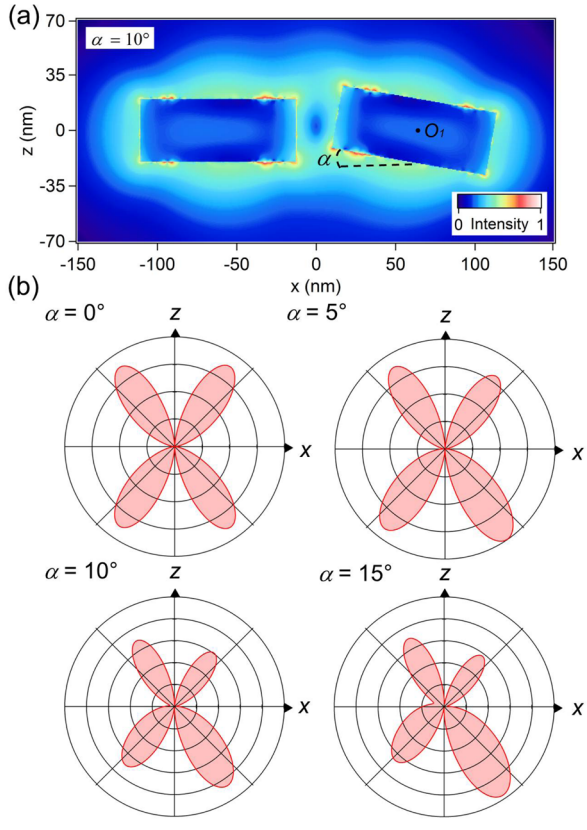

Figure 7. (a) Near-field distribution of the second harmonic intensity (shown in a logarithmic scale) close to a tilted nanoantenna. The arm is turned around the (O_1, *y*)-axis by a rotation angle α. (b) Normalized second harmonic intensity scattered in the vertical plane as a function of the detection angle calculated considering the second harmonic scattered wave polarized into the (O, *x*, *z*) plane. Results obtained for different values of α are shown.

dx.doi.org/10.1021/nl400393e | *Nano Lett.* 2013, 13, 1787−1792

arm tilt increases, the SH emission pattern evolves from a perfectly symmetric four lobe pattern, as expected for a symmetric antenna, to an asymmetric one, as observed in the case of the realistic optical antenna. Interestingly, a small rotation angle ($\alpha = 5°$) leads to a non-negligible variation of the lobe magnitudes (18%), demonstrating that SHG is sensitive to small defects in the nanoantennas geometry. For the corresponding linear signal, a dipolar emission is still observed (see Figure 3). Another plausible defect in the nanoantenna geometry is the misalignment of the arms. Results considering a shift of the nanoantenna arm positions along the z-direction are shown in Figure 8. The shift is quantified by the distance e

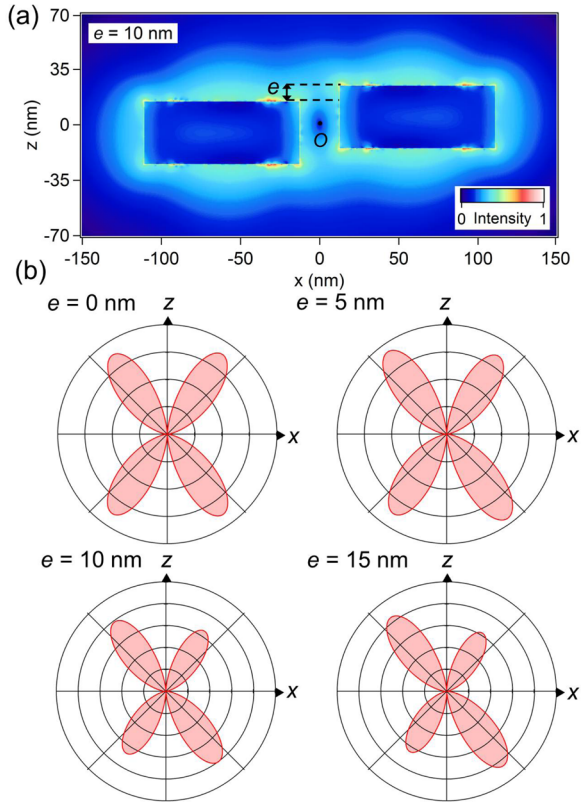

Figure 8. (a) Near-field distribution of the second harmonic intensity (shown in a logarithmic scale) close to a misaligned nanoantenna. The position of the nanoantenna arms is shifted along the z-axis. e denotes the side-to-side distance. (b) Normalized second harmonic intensity scattered in the vertical plane as a function of the detection angle calculated considering the second harmonic scattered wave polarized into the (O, x, z) plane. Results obtained for different values of e are shown.

(Figure 8a). The normalized SH intensity scattered in the vertical plane as a function of the detection angle calculated considering the SH scattered wave polarized into the (O, x, z) plan is shown for values of the side-to-side distance e between 0 and 15 nm. The variation of the lobe magnitudes increases from 8% for a side-to-side distance e = 5 nm to 35% for e = 15 nm, demonstrating that SHG is also extremely sensitive to arms misalignments. Contrary to the cases of the realistic and tilted antennas, the opposite lobes have the same magnitudes in the case of a misaligned nanoantenna. This is expected since the misaligned nanostructure is still invariant by a 180° rotation around the (O, y)-axis. Hence, SHG enables the discrimination of the impact of the misaligned arms on the nanoantenna optical properties with the impact of other fabrication defects. Supporting Information Figure S5 shows that, even if the impact of a 15° tilted arm or of a nanodefect on the lateral side are almost the same considering the second harmonic scattered wave polarized in the (O, x, z) plane, this is not the case considering the SH scattered wave polarized in the (O, x, y) plane. Indeed, a 15° tilted arm leads to a 10% variation of the lobe magnitudes while the two lobes remain perfectly symmetric in the case of a nanodefect on the lateral side. These results clearly demonstrate that, although a complete retrieval of the nanoantenna shape is not possible, SHG can be used as a sensitive tool for in situ optical characterization of nanoantennas. For example, SHG enables the rapid screening of a nanoantenna array to determine which structures are "defect-free". This cannot be performed in the linear optics regime, where a minute geometry asymmetry or surface roughness do not no impact the scattering pattern (see Figure 3).

Let us finally address further experimental issues. The results discussed in this letter show unambiguously that angular-resolved SHG is an efficient way to optically characterize the morphology of nanoantennas. Such an experiment has been already performed in the case of gold nanorod arrays.[55] Furthermore, SHG from single antennas has been observed, indicating that the SH cross section is high enough for studying a single antenna.[23,24] Another experimental issue is the heating of the nanostructure under strong light illumination.[56] The observation of nonlinear optical processes requires the use of ultrashort laser sources and resonating absorption at the fundamental wavelength can result in nanostructure damages. We have performed complementary simulations considering a fundamental wavelength λ = 800 nm, which corresponds to the operating wavelength of the majority of available femtosecond laser sources. This excitation wavelength is far from any resonances of the considered nanoantennas. Yet, as in the resonant case, the asymmetry of the realistic nanoantenna is clearly revealed in off-resonant SHG, showing the flexibility of SHG as a tool for the optical characterization of nanoantennas.

In summary, the optical response of gold nanoantennas has been studied using SIE methods. The linear response has been considered first showing that the far-field properties are barely affected by the quality and the symmetry of the structure. On the other hand, the SHG has been found to be highly sensitive to the nanoantenna morphology, even when the linear properties are almost identical. Interestingly, extremely small defects in the arm shape or nanoantenna geometry are clearly revealed by SHG far-field analysis, demonstrating that SHG is a promising tool for sensitive optical characterization of plasmonic nanoantennas. It should be emphasized that defects located where the linear field is strong (e.g., in the antenna gap) do not necessarily have the strongest impact on the SH signal. This work paves the way for future investigations of SHG from more complicated optical antennas, such as circuit loaded nanoantennas.[57,58] We also expect that nonlinear optical processes from nanoantennas for which quantum mechanical effects have to be taken into account will also be of particular interest in the future.[59−62]

■ ASSOCIATED CONTENT

Ⓢ Supporting Information

Additional information and figures. This material is available free of charge via the Internet at http://pubs.acs.org.

dx.doi.org/10.1021/nl400393e | Nano Lett. 2013, 13, 1787−1792

AUTHOR INFORMATION

Corresponding Author

*E-mail: jeremy.butet@epfl.ch.

Notes

The authors declare no competing financial interest.

ACKNOWLEDGMENTS

Funding from the Swiss National Science Foundation (SNSF, Project 200021_132694) is gratefully acknowledged.

REFERENCES

(1) Maier, S. A. *Plasmonics: Fundamentals and Applications*; Springer: New York, 2007.
(2) Prodan, E.; Radloff, C.; Halas, N. J.; Nordlander, P. *Science* **2003**, *302*, 419−422.
(3) Halas, N. J.; Lal, S.; Chanq, W.-S.; Link, S.; Nordlander, P. *Chem. Rev.* **2011**, *111*, 3913−3961.
(4) Mühlschlegel, P.; Eisler, H.-J.; Martin, O. J. F.; Hecht, B.; Pohl, D. W. *Science* **2005**, *308*, 1607−1608.
(5) Novotny, L.; van Hulst, N. F. *Nat. Photonics* **2011**, *5*, 83−90.
(6) Biagioni, P.; Huang, J.-S.; Hecht, B. *Rep. Prog. Phys.* **2012**, *75*, 024402.
(7) Fischer, H.; Martin, O. J. F. *Opt. Express* **2008**, *16*, 9144−9154.
(8) Taminiau, T. H.; Stefani, F. D.; van Hulst, N. F. *Nano Lett.* **2011**, *11*, 1020−1024.
(9) Farahani, J. N.; Pohl, D. W.; Eisler, H.-J.; Hecht, B. *Phys. Rev. Lett.* **2005**, *95*, 017402.
(10) Curto, A. G.; Volpe, G.; Taminiau, T. H.; Kreuzer, M. P.; Quidant, R.; van Hulst, N. F. *Science* **2010**, *329*, 930−933.
(11) Ward, D. R.; Grady, N. K.; Levin, C. S.; Halas, N. J.; Wu, Y.; Nordlander, P.; Natelson, D. *Nano Lett.* **2007**, *7*, 1396−1400.
(12) Zhang, W.; Fischer, H.; Schmid, T.; Zenobi, R.; Martin, O. J. F. *J. Phys. Chem. C* **2009**, *113*, 14672−14675.
(13) Kern, A. M.; Meixner, A. J.; Martin, O. J. F. *ACS Nano* **2012**, *6*, 9828−9836.
(14) Zhu, W.; Wang, D.; Crozier, K. B. *Nano Lett.* **2012**, *12*, 6235−6243.
(15) Knight, M. W.; Liu, L.; Wang, Y.; Brown, L.; Mukherjee, S.; King, N. S.; Everitt, H. O.; Nordlander, P.; Halas, N. J. *Nano Lett.* **2012**, *12*, 6000−6004.
(16) Dombi, P.; Hörl, A.; Rácz, I.; Márton, I.; Trügler, A.; Krenn, J. R.; Hohenester, U. *Nano Lett.* **2013**, *13* (2), 674−678.
(17) Juan, M. L.; Righini, M.; Quidant, R. *Nat. Photonics* **2011**, *5*, 349−356.
(18) Zhang, W. H.; Huang, L. N.; Santschi, C.; Martin, O. J. F. *Nano Lett.* **2010**, *10*, 1006−1011.
(19) Kauranen, M.; Zayats, A. V. *Nat. Photonics* **2012**, *6*, 737−748.
(20) Castro-Lopez, M.; Brinks, D.; Sapienza, R.; van Hulst, N. F. *Nano Lett.* **2011**, *11*, 4674−4678.
(21) Biagioni, P.; Brida, D.; Huang, J.-S.; Kern, J.; Duo, L.; Hecht, B.; Finazzi, M.; Cerullo, G. *Nano Lett.* **2012**, *12*, 2941−2947.
(22) Ko, K. D.; Kumar, A.; Fung, K. H.; Ambekar, R.; Liu, G. L.; Fang, N. X.; Kimani, J.; Toussaint, C. *Nano Lett.* **2011**, *11*, 61−65.
(23) Slablab, A.; Le Xuan, L.; Zielinski, M.; de Wilde, Y.; Jacques, V.; Chauvat, D.; Roch, J.-F. *Opt. Express* **2012**, *20*, 220−227.
(24) Hanke, T.; Krauss, G.; Träutlein, D.; Wild, B.; Bratschitsch, R.; Leitenstorfer, A. *Phys. Rev. Lett.* **2009**, *103*, 257404.
(25) Hentschel, M.; Utikal, T.; Giessen, H.; Lippitz, M. *Nano Lett.* **2012**, *12*, 3778−3782.
(26) Navarro-Cia, M.; Maier, S. A. *ACS Nano* **2012**, *6*, 3537−3544.
(27) Kim, S.; Jin, J.; Kim, Y.-J.; Park, I.-Y.; Kim, Y.; Kim, S.-W. *Nature* **2008**, *453*, 757−760.
(28) Danckwerts, M.; Novotny, L. *Phys. Rev. Lett.* **2007**, *98*, 026104.
(29) Abb, M.; Albella, P.; Aizpurua, J.; Muskens, O. L. *Nano Lett.* **2011**, *11*, 2457−2463.
(30) Schumacher, T.; Kratzer, K.; Molnar, D.; Hentschel, M.; Giessen, H.; Lippitz, M. *Nat. Commun.* **2011**, *2*, 333.
(31) Harutyunyan, H.; Volpe, G.; Quidant, R.; Novotny, L. *Phys. Rev. Lett.* **2012**, *108*, 217403.
(32) Thyagarajan, K.; Rivier, S.; Lovera, A.; Martin, O. J. F. *Opt. Express* **2012**, *20*, 12860−12865.
(33) Aouani, H.; Navarro-Cia, M.; Rahmani, M.; Sidiropoulos, T. P. H.; Hong, M.; Oulton, R. F.; Maier, S. A. *Nano Lett.* **2012**, *12*, 4997−5002.
(34) Butet, J.; Duboisset, J.; Bachelier, G.; Russier-Antoine, I.; Benichou, E.; Jonin, C.; Brevet, P.-F. *Nano Lett.* **2010**, *10*, 1717−1721.
(35) Valev, V. K.; Silhanek, A. V.; Verellen, N.; Gillijns, W.; Van Dorpe, P.; Aktsipetrov, O. A.; Vandenbosch, G. A. E.; Moshchalkov, V. V.; Verbiest, T. *Phys. Rev. Lett.* **2010**, *104*, 127401.
(36) Zhang, Y.; Grady, N. K.; Ayala-Orozco, C.; Halas, N. J. *Nano Lett.* **2011**, *11*, 5519−5523.
(37) Bouhelier, A.; Beversluis, M.; Hartschuch, A.; Novotny, L. *Phys. Rev. Lett.* **2003**, *90*, 013903.
(38) Husu, H.; Siikanen, R.; Mäkitalo, J.; Lehtolahti, J.; Laukkanen, J.; Kuittinen, M.; Kauranen, M. *Nano Lett.* **2012**, *12*, 673−677.
(39) Bautista, G.; Huttunen, M. J.; Mäkitalo, J.; Kontio, J. M.; Simonen, J.; Kauranen, M. *Nano Lett.* **2012**, *12*, 3207−3212.
(40) Centini, M.; Benedetti, A.; Sibilia, C.; Bertolotti, M. *Opt. Express* **2011**, *19*, 8218−8232.
(41) Berthelot, J.; Bachelier, G.; Song, M.; Rai, P.; Colas des Francs, G.; Dereux, A.; Bouhelier, A. *Opt. Express* **2012**, *20*, 10498−10508.
(42) Canfield, B. K.; Husu, H.; Laukkanen, J.; Bai, B. F.; Kuittinen, M.; Turunen, J.; Kauranen, M. *Nano Lett.* **2007**, *7*, 1251−1255.
(43) Butet, J.; Russier-Antoine, I.; Jonin, C.; Lascoux, N.; Benichou, E.; Brevet, P.-F. *Nano Lett.* **2012**, *12*, 1697−1701.
(44) Kern, A. M.; Martin, O. J. F. *Nano Lett.* **2011**, *11*, 482−487.
(45) Kern, A. M.; Martin, O. J. F. *J. Opt. Soc. Am. A* **2009**, *26*, 732−740.
(46) Kern, A. M.; Martin, O. J. F. *IEEE Trans. Antennas Propag.* **2010**, *58*, 2158−2161.
(47) Johnson, P. B.; Christy, R. W. *Phys. Rev. B* **1972**, *6*, 4370−4379.
(48) Boyd, R. W. *Nonlinear optics*; Academic Press: New York, 1992.
(49) Mäkitalo, J.; Suuriniemi, S.; Kauranen, M. *Opt. Express* **2011**, *19*, 23386−23399.
(50) Bachelier, G.; Butet, J.; Russier-Antoine, I.; Jonin, C.; Benichou, E.; Brevet, P.-F. *Phys. Rev. B* **2010**, *82*, 235403.
(51) Wang, F. X.; Rodríguez, F. J.; Albers, W. M.; Ahorinta, R.; Sipe, J. E.; Kauranen, M. *Phys. Rev. B* **2009**, *80*, 233402.
(52) Butet, J.; Bachelier, G.; Russier-Antoine, I.; Jonin, C.; Benichou, E.; Brevet, P.-F. *Phys. Rev. Lett.* **2010**, *105*, 077401.
(53) Dadap, J. I.; Shan, J.; Eisenthal, K. B.; Heinz, T. F. *Phys. Rev. Lett.* **1999**, *83*, 4045−4048.
(54) Bachelier, G.; Russier-Antoine, I.; Benichou, E.; Jonin, C.; Brevet, P.-F. *J. Opt. Soc. Am. B* **2008**, *25*, 955−960.
(55) McMahon, M. D.; Lopez, R.; Haglund, R. F., Jr; Ra, E. A.; Bunton, P. H. *Phys. Rev. B* **2006**, *73*, 041401.
(56) Baffou, G.; Rigneault, H. *Phys. Rev. B* **2011**, *84*, 035415.
(57) Liu, N.; Wen, F.; Zhao, Y.; Wang, Y.; Nordlander, P.; Halas, N. J.; Alù, A. *Nano Lett.* **2013**, *13*, 142−147.
(58) Alù, A.; Engheta, N. *Nat. Photonics* **2008**, *2*, 307−309.
(59) Savage, K. J.; Hawkeye, M. M.; Esteban, R.; Borisov, A. G.; Aizpurua, J.; Baumberg, J. J. *Nature* **2012**, *491*, 574−577.
(60) McMahon, J. M.; Gray, S. K.; Schatz, G. C. *Nano Lett.* **2010**, *10*, 3473−3481.
(61) Zuloaga, J.; Prodan, E.; Nordlander, P. *Nano Lett.* **2009**, *9*, 887−891.
(62) Marinica, D. C.; Kazansky, A. K.; Nordlander, P.; Aizpurua, J.; Borisov, A. G. *Nano Lett.* **2012**, *12*, 1333−1339.